Hindawi
Journal of Nanomaterials
Volume 2022, Article ID 8630685, 11 pages
https://doi.org/10.1155/2022/8630685

Research Article

Zinc/Cobalt-Based Zeolite Imidazolate Frameworks for Simultaneously Degrading Dye and Inhibiting Bacteria

Nguyen Thi Thanh Tu,[1] **Lu Hoang Khang**,[1] **Nguyen Ngoc Phuong Thao**,[1] **Nguyen Thi Thu Hien**,[2] **Thuy Chau To**,[2] **Le Thi Hong Diep**,[3] **Le Van Thanh Son**,[4] **Phan Lien**,[4] **Vo Thang Nguyen**,[4] **and Dinh Quang Khieu**[5]

[1]*Faculty of Applied Technology, School of Engineering and Technology, Van Lang University, 700000, Vietnam*
[2]*Thu Dau Mot University, Binh Duong 75000, Vietnam*
[3]*Faculty of Environmental & Food Engineering, Nguyen Tat Thanh University, 700000, Vietnam*
[4]*University of Education and Science, The University of Danang, 500000, Vietnam*
[5]*University of Sciences, Hue University, 530000, Vietnam*

Correspondence should be addressed to Nguyen Thi Thanh Tu; tu.ntt@vlu.edu.vn
and Dinh Quang Khieu; dqkhieu@hueuni.edu.vn

Received 4 May 2022; Revised 25 August 2022; Accepted 15 September 2022; Published 30 September 2022

Academic Editor: Mai Duy Hien

In this work, the zinc/cobalt-based zeolite imidazolate frameworks ((Co/Zn)ZIFs) were synthesized with the solvothermal method. The obtained material was characterized by utilizing scanning electron microscopy (SEM), X-ray diffraction (XRD), UV-Vis diffusive reflectance spectroscopy, and nitrogen adsorption-desorption isotherms. XRD and SEM analyses show that (Co/Zn)ZIFs are composed of nanocrystals with polyhedral shapes of around 50–100 nm and belong to the I-43m space group as those of ZIF-8 and ZIF-67. Optical studies demonstrate a red shift in the absorbance spectrum of (Co/Zn)ZIFs compared with individual components of ZIF-67 or ZIF-8. (Co/Zn)ZIF composite was utilized as photocatalytic material to treat a model aqueous solution containing rhodamine B and bacteria. It was found that (Co/Zn)ZIFs could simultaneously degrade rhodamine B and inhibit bacteria (*E. coli* and *S. aureus*). The manufactured composite could catalyze the mineralization of rhodamine B and also exhibited good antibacterial activity against Gram-negative *E. coli* (93.32% inhibition rate) and Gram-positive *S. aureus* (90.86% inhibition rate) in the visible-light region within four hours of irradiation. Gram-negative bacteria were more resistant to (Co/Zn)ZIFs than Gram-positive bacteria. (Co/Zn)ZIFs can be used as light-driven catalysts for water and environmental detoxification from organic compounds like dyes and bacteria.

1. Introduction

The rapid development of industrialization in recent years has contributed to significant economic growth. At the same time, environmental pollution is also at an alarming level, affecting the living environment of humans and animals. In particular, wastewater from industrial production facilities, especially wastewater from textile dyeing factories, poses a severe threat to the environment. The presence of dyes in wastewater is a major concern because of their toxicity and unaesthetic that can cause adverse effects on biological life, including cancer and genetic mutations [1–3]. In addition, the presence of bacteria in water also affects the environment, especially strains of enterobacteria and Gram-negative, anaerobic bacteria, including *Escherichia coli* (*E. coli*), being able to cause diseases on the digestive tract in humans and animals. Therefore, developing friendly and effective techniques to degrade dyes and, at the same time, disinfect wastewater has become a vital and urgent issue in environmental protection. Numerous techniques for separate treatment of dyes or bacteria have been reported. Physicochemical methods have been developed to treat dye wastewater, such as

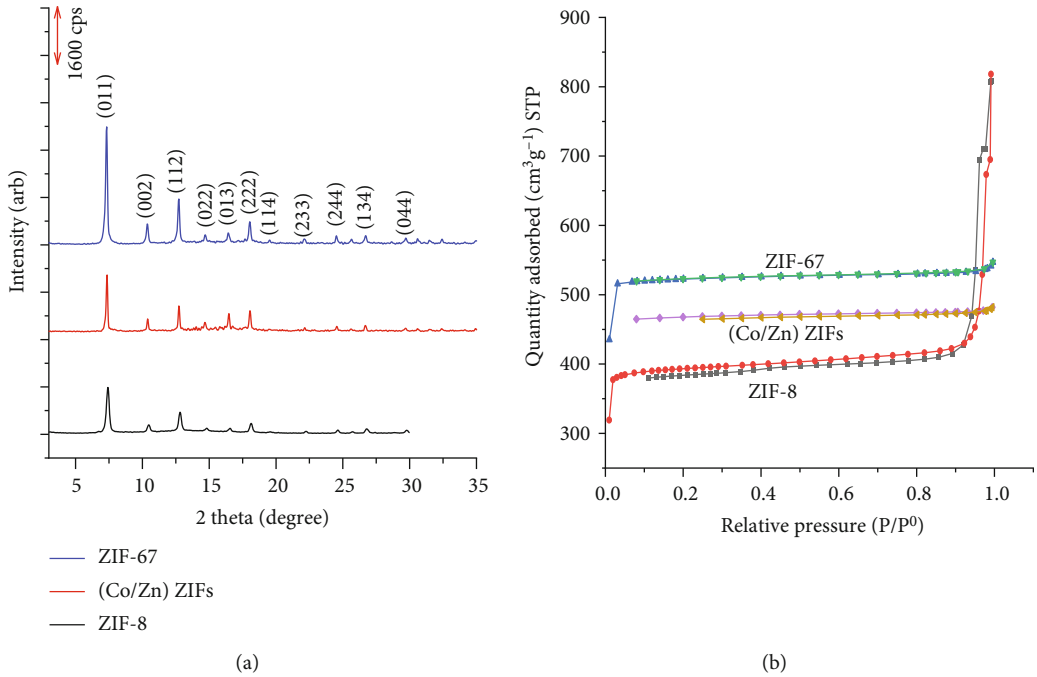

Figure 1: (a) XRD diagram and (b) nitrogen adsorption and desorption isotherms of ZIF-67, ZIF-8, and (Co/Zn)ZIFs.

biochemical oxidation [4], adsorption [5–7], ion exchange [8, 9], photocatalysis [10, 11], and advanced oxidation [12]. Recently, several oxide or metal nanoparticles exhibiting antibacterial activity or both antibacterial and organic compound degradation activities have been reported. Nair et al. addressed the antibacterial activity of ZnO- and Co-doped ZnO nanoparticles on Gram-positive and Gram-negative bacteria [13]. Valerini et al. presented that Ag-coated polycaprolactone exhibited an excellent antibacterial action against *E. coli* [14]. In another study, Rao et al. found that Ag nanoparticles/g-C_3N_4 nanosheets showed efficient photocatalytic and antibacterial performance [15].

ZIFs (zeolitic imidazole frameworks) are a class of metal-organic frameworks (MOFs) formed from tetrahedral divalent cations ($M^{2+} = Zn^{2+}$ or Co^{2+}) with imidazolate ligands [16, 17]. Most ZIFs have a large bandgap energy (E_g); for example, E_g of ZIF-67 and ZIF-8 is 4.3 and 5.3 eV [18]. Therefore, reducing E_g to improve the photocatalytic performance of ZIFs in the visible-light region is essential and has practical significance. Chen et al. [19] reported that ZnO/ZIF-8 was an effective photocatalyst for completely degrading methylene blue. Yang et al. [20] added Cu to ZIF-67 to promote the catalytic activity of Cu/ZIF-67 for methyl orange decomposition in the visible-light region. Zhou et al. [17] synthesized ZIFs based on Zn/Co for the first time with improved chemical properties compared with single ZIF-8 or ZIF-67. Taheri et al. reported the antibacterial activity of ZIF-8 for *E. coli* [21]. According to our best knowledge, research on the photocatalytic activity of this kind of material for simultaneously degrading dyes and inhibiting bacteria is less available. Therefore, developments of ZIFs with antimicrobial properties are of considerable interest. In the present study, we present the synthesis of (Co/Zn)ZIFs with the hydrothermal method and the photocatalytic activity toward rhodamine B. The antimicrobial activity of (Co/Zn)ZIFs against *E. coli* ATCC 25922 (Gram-negative) and *S. aureus* ATCC 25923 (Gram-positive) in aqueous solutions was also addressed.

2. Experimental

2.1. Materials. Cobalt nitrate ($Co(NO_3)_2{\cdot}6H_2O$, Deajung, Korea), 2-methylimidazole ($C_4H_6N_2$, Sigma, USA) (Hmim), methanol (CH_3OH, Guangzhou, China), ethanol (C_2H_5OH, Guangzhou, China), zinc nitrate ($Zn(NO_3)_2{\cdot}6H_2O$, Deajung, Korea), and rhodamine B ($C_{28}H_{31}ClN_2O_3$, denoted RhB) were used in the study.

2.2. Preparation of ZIF-8, ZIF-67, and (Co/Zn)ZIFs. ZIF-8, ZIF-67, and (Co/Zn)ZIFs were synthesized according to references [22, 23]. For ZIF-67, 1.164 g of $Co(NO_3)_2{\cdot}6H_2O$ and 1.312 g of 2-methylimidazole were dissolved in 100 mL of CH_3OH. The mixture was placed in a Teflon autoclave and kept in an oven at 150°C for 5 h. The product was then centrifuged for 15 min (1500 rpm). The obtained solid was rinsed three times with ethanol. Then, the resulting purple solid was dried at 120°C for about 24 h to obtain the ZIF-67. ZIF-8 was synthesized with the same procedure with $Zn(NO_3)_2{\cdot}6H_2O$ (1.188 g). A series of (Co/Zn)ZIFs with different molar Co/Zn ratios (1 : 9), (2 : 8), (3 : 7), (5 : 5), (6 : 4), and (7 : 3) was synthesized in a similar manner by using a mixture of $Co(NO_3)_2{\cdot}6H_2O$ and $Zn(NO_3)_2{\cdot}6H_2O$. In a preliminary test, (Co/Zn)ZIFs with Co/Zn molar ratio of 6/4 exhibit high photocatalytic and antibacterial activity; therefore, this material was selected for further experiments (Table S1).

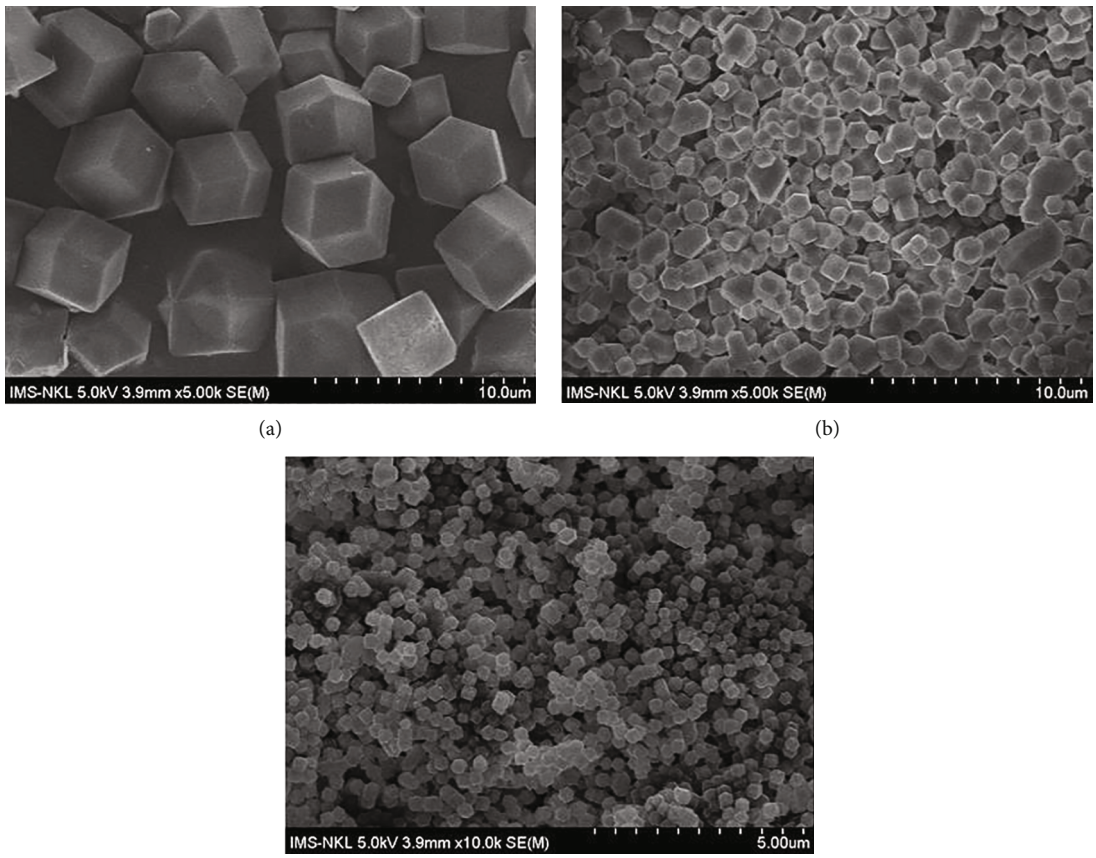

Figure 2: SEM images of ZIF-67 (a), ZIF-8 (b), and (Co/Zn)ZIFs (c).

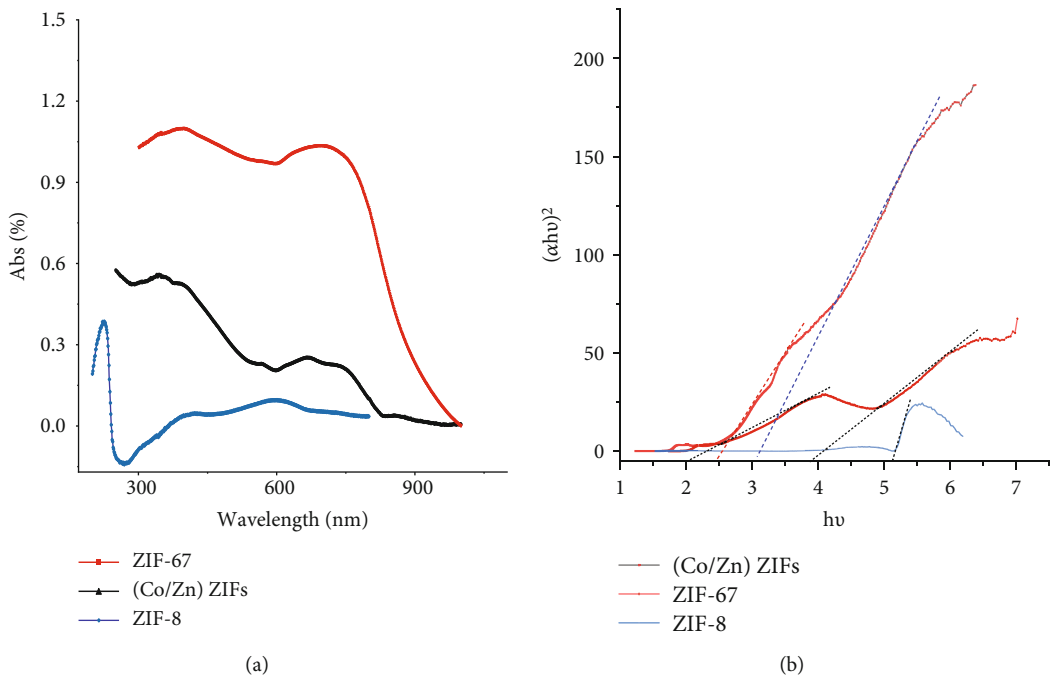

Figure 3: UV-Vis DRS spectra (a) and Tauc's plots of (Co/Zn)ZIFs, ZIF-67, and ZIF-8 (b).

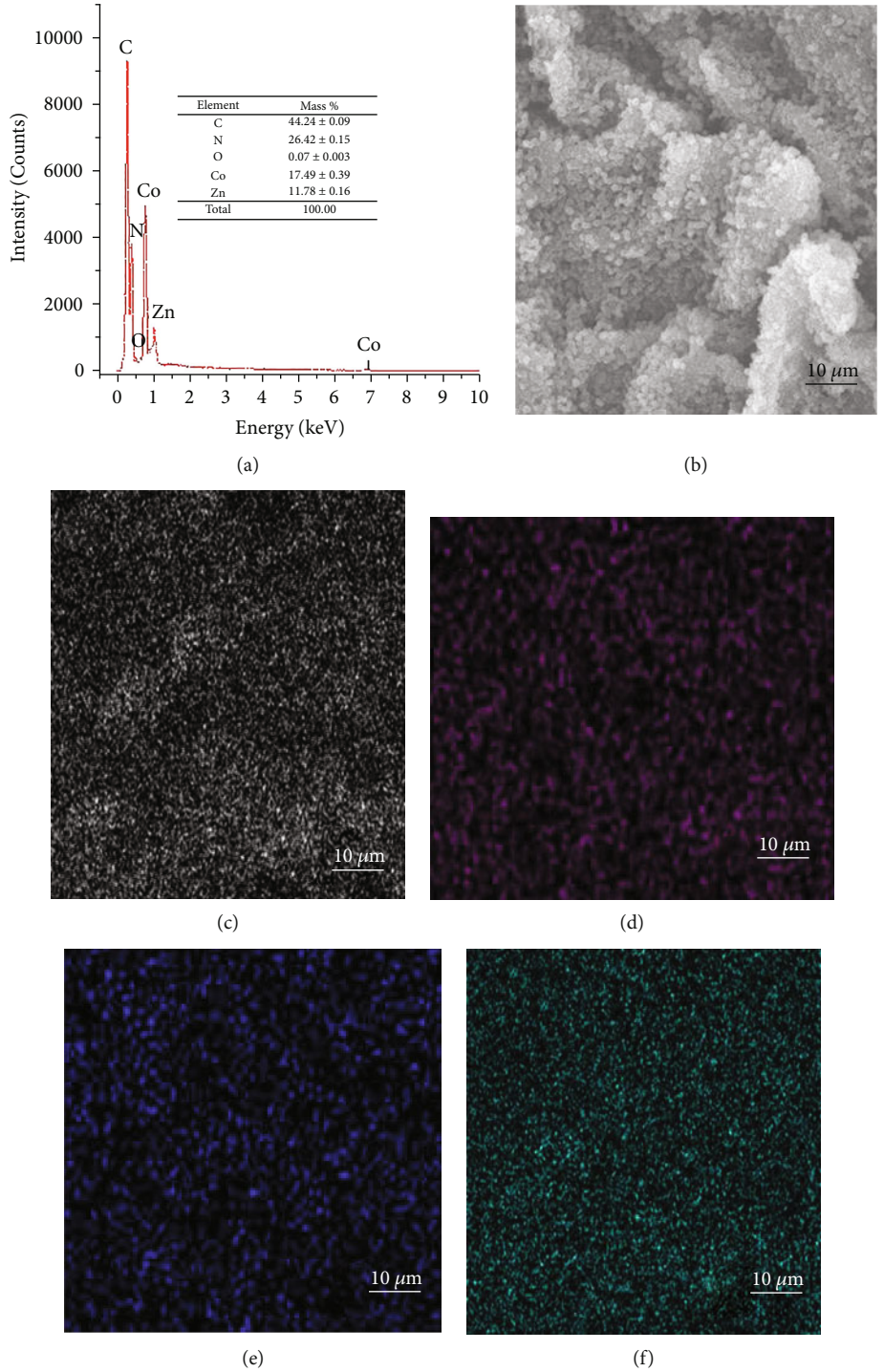

Figure 4: EDX spectrum of (Co/Zn)ZIFs (a), SEM image (b), carbon mapping (c), nitrogen mapping (d), cobalt mapping (e), and zinc mapping (f).

2.3. Apparatus. The powder X-ray diffraction (XRD) was performed on D8 Advance, Bruker (Germany). The morphology of ZIF-8, ZIF-67, and (Co/Zn)ZIFs was observed from scanning electron microscopy (SEM JMS-5300LV, Japan) images. Textural properties were investigated by means of nitrogen adsorption-desorption isotherms (Micrometrics TriStar 3000 at 77 K). The elemental composition of samples was detected by EDX mapping (JSM-IT200 InTouchScope). UV-Vis spectroscopy was measured by using a Lambda 25 Spectrophotometer-Perkin Elmer at λ_{max} of RhB (553 nm). Total organic carbon (TOC) was measured on TOC-VCPH/CP (Shimadzu).

2.4. Bacterial Strains and Growing Conditions. Gram (–) *Escherichia coli* ATCC 25922 (*E. coli*) and Gram (+) *Staphylococcus aureus* ATCC 25923 (*S. aureus*) were used to study

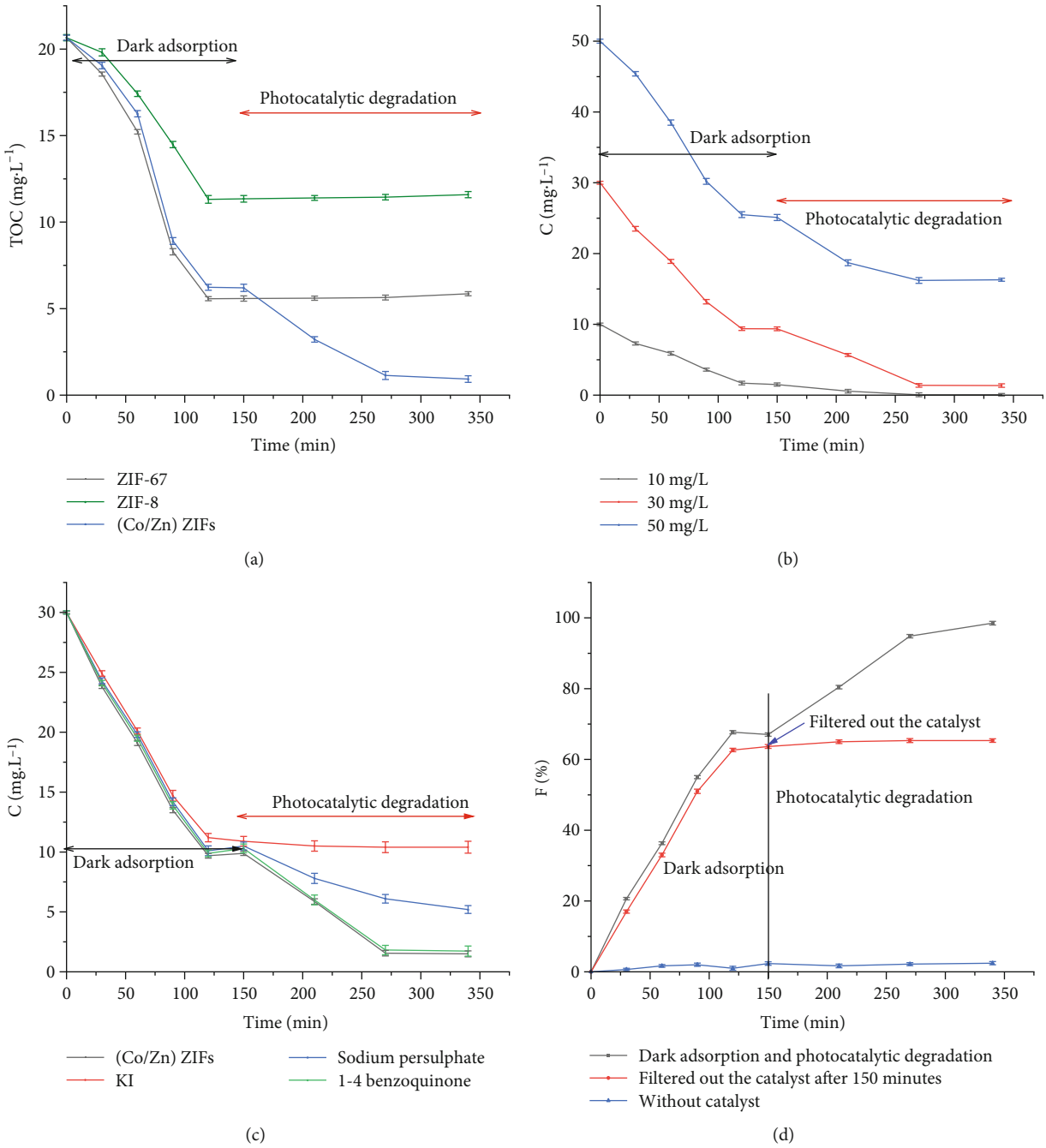

Figure 5: (a) Visible light-driven photocatalytic degradation of RhB on different ZIF materials (experimental condition: $V = 1000$ mL; the initial concentration is from 30 mg·L^{-1}; the adsorbent mass is 0.1 g) and (b) kinetics of decolorization on (Co/Zn)ZIFs (experimental condition: $V = 1000$ mL; the initial concentration is from 10, 30, and 50 mg·L^{-1}; the adsorbent mass is 0.1 g). (c) Effect of photogenerated carrier scavenger on photodegradation of RhB. (d) Leaching (experimental conditions: $V = 1000$ mL, mass of catalyst = 0.1 g, dark adsorption in 150 min, and photodegradation in 340 min).

the antibacterial activity of the synthesized products. The *E. coli* strain culture was grown in LB (Luria–Bertani) broth, and *S. aureus* was grown in TS (tryptic soy) broth.

2.5. Visible-Light-Derived Photocatalytic Activity for RhB Degradation and Antibacterial Activity against E. coli and S. aureus with (Co/Zn)ZIFs. 0.1 g of each ZIF-67, ZIF-8, and (Co/Zn)ZIF material was placed into a 1000 mL beaker containing 500 mL of RhB solution (30 mg·L^{-1}) and *E. coli* and *S. aureus* strains (10^6–10^7 CFU·mL^{-1}). The beakers were sealed and placed in the dark to prevent light exposure, and the mixture was stirred with a magnetic stirrer for 120 min to reach adsorption/desorption equilibrium. Then, an Osram 160 W filament lamp (filter cutoff $\lambda < 420$ nm) illuminated the resulting suspension. 5 mL of suspension was withdrawn at defined intervals and then centrifuged to remove the solid. The mineralization degree of RhB in the supernatant was estimated with the total organic carbon

measurement. Each experiment was repeated three times. Simultaneously, 100 μL of the solution was taken, diluted 10,000 times, and spread on LB or TSB agar plates (incubated at 37°C; the number of colonies was recorded after 24 h to assess the antibacterial activity of the material via the plate spread method).

The antibacterial rate was utilized to assess the antibacterial activity according to the following equation:

$$H\,(\%) = \frac{C_{CS} - C_{SS}}{C_{CS}} \times 100\%, \quad (1)$$

where C_{SS} and C_{CS} are the bacterial population of the survey and control samples (CFU·mL^{-1}).

The kinetics study was performed in a similar manner on RhB solution at initial concentrations of 10, 30, and 50 ppm. The concentration of remaining RhB in the supernatant was determined with a UV-Vis adsorption spectroscope at λ_{max} equal to 553 nm.

3. Results and Discussion

3.1. Characterization of Materials. Figure 1 shows the XRD patterns of the ZIF-67, ZIF-8, and (Co/Zn)ZIF samples. The spatial distances d of the faces (011), (002), (112), (022), (113), (222), and (114) of ZIF-8 or ZIF-67 are in good agreement with those reported previously [17, 24–26]. Since both ZIF-67 and ZIF-8 crystallize in the crystal system I-43m [20], the diffraction peaks of (Co/Zn)ZIFs are observed at the same 2θ as ZIF-67 and ZIF-8 with an intermediate intensity between ZIF-67 and ZIF-8. The surface area and pore properties of the materials were investigated by measuring nitrogen adsorption and desorption at 77 K (Figure 1(b)). The adsorption and desorption isotherms follow the type I according to the IUPAC classification. All samples have a microporous structure. However, the isotherm of ZIF-8 rises remarkably at high relative pressures, indicating that a mesoporous capillary system was formed between the particles.

The BET-specific surface area of ZIF-67, ZIF-67, and (Co/Zn)ZIFs calculated from the N_2 adsorption and desorption isotherm is 1530, 1176, and 1325 $m^2 \cdot g^{-1}$, respectively. The pore size distribution calculated from the Barrett-Joyner-Halenda model shows that ZIF-67 and (Co/Zn)ZIFs have almost the same pore width (around 20 Å), indicating their structural similarities. In addition, the adsorption on (Co/Zn)ZIFS is fast with saturation at a relative pressure of less than 0.1, confirming its microporous structure, analogous to ZIF.

The morphology of ZIF-67, ZIF-8, and (Co/Zn)ZIFs is presented in Figure 2. While ZIF-67 consists of polyhedron particles with a diameter ranging from 200 to 500 nm, (Co/Zn)ZIFs retain the polyhedral morphology of ZIF-67, yet with a smaller size (50–200 nm).

To assess the optical absorption capacity of the as-prepared ZIFs, we calculated the bandgap (E_g) of the material by using UV–Vis diffuse reflection spectroscopy (Figure 3(a)). The bandgap of a material can be obtained from the Kubelka–Munk function formula.

Table 1: A comparison of rate coefficient of (Co/Zn)ZIFs with other previously reported materials.

Catalyst	C_{RhB} (mg·L^{-1})	k_r (min^{-1})	Reference
$BiVO_4$	5	0.00102	[30]
CuO–ZrO_2	10	0.0006	[31]
ZnO	5	0.0028	[32]
CuO	5	0.0203	[32]
ZnO/CuO	5	0.0326	[32]
(ZnO/CuO)/rGO	5	0.0627	[32]
ZnO	5	0.0203	[33]
ZnO/g–C_3N_4	5	0.0284	[33]
(Co/Zn)ZIFs	10	0.028	This work
(Co/Zn)ZIFs	30	0.016	This work
(Co/Zn)ZIFs	50	0.004	This work

$$\alpha \times h \times \nu = A \times \left(h \times \nu - E_g\right)^{n/2}, \quad (2)$$

where α, h, ν, A, and E_g are the absorption coefficient, Plank's constant, light frequency, proportionality constant, and bandgap energy, respectively; $n = 1$ and 4, corresponding to direct and indirect bandgap semiconductors. Figure 3(b) presents the fitting diagram of $(\alpha \times h \times \nu)^2$ vs. $h \times \nu$ for the indirect bandgap [27]. Thus, extrapolating the linear region to the abscissa yields the bandgap energy of the material. Two bandgaps are found at 2.05 and 3.98 eV for ZIF-67, while only one bandgap is around 5.18 eV for ZIF-8. (Co/Zn)ZIFs have two bandgaps at around 2.45 and 3.05 eV. The high bandgap energy at 5.18 and 3.98 eV for ZIF-8 and ZIF-67 can mainly be attributed to the charge transfer between the ligand and the metals [28]. The low bandgap of ZIF-67 (2.05 eV), corresponding to the characteristic absorption band at 500–650 nm, is attributed to the typical d - d transition in tetrahedral cobalt [29]. Furthermore, the bandgap of (Co/Zn)ZIFs is lower than that of ZIF-8 or ZIF-67, indicating that the combination of Co and Zn reduces the energy required for optical transition and can promote its photocatalytic activity.

The distribution of the elements in the composite was studied with EDX mapping (Figure 4). As expected, the EDX spectrum shows the presence of five elements: Zn (11.78%), Co (17.49%), C (44.24%), O (0.07%), and N (26.42%). The elements randomly disperse throughout the sample surface, indicating the composite homogeneous phase.

3.2. Rhodamine B Degradation and Antibacterial Activity of ZIF-67, ZIF-8, and (Co/Zn)ZIFs. The elimination of RhB with ZIF-67, ZIF-8, and (Co/Zn)ZIFs might occur in two steps: adsorption and photocatalytic degradation. The ability to eliminate RhB was evaluated *via* the decrease of TOC, which is expressed as elimination efficiency (F)

$$F = \frac{100 * (C_0 - C_t)}{C_0}, \quad (3)$$

where C_0 is the initial TOC and C_t is TOC at time t.

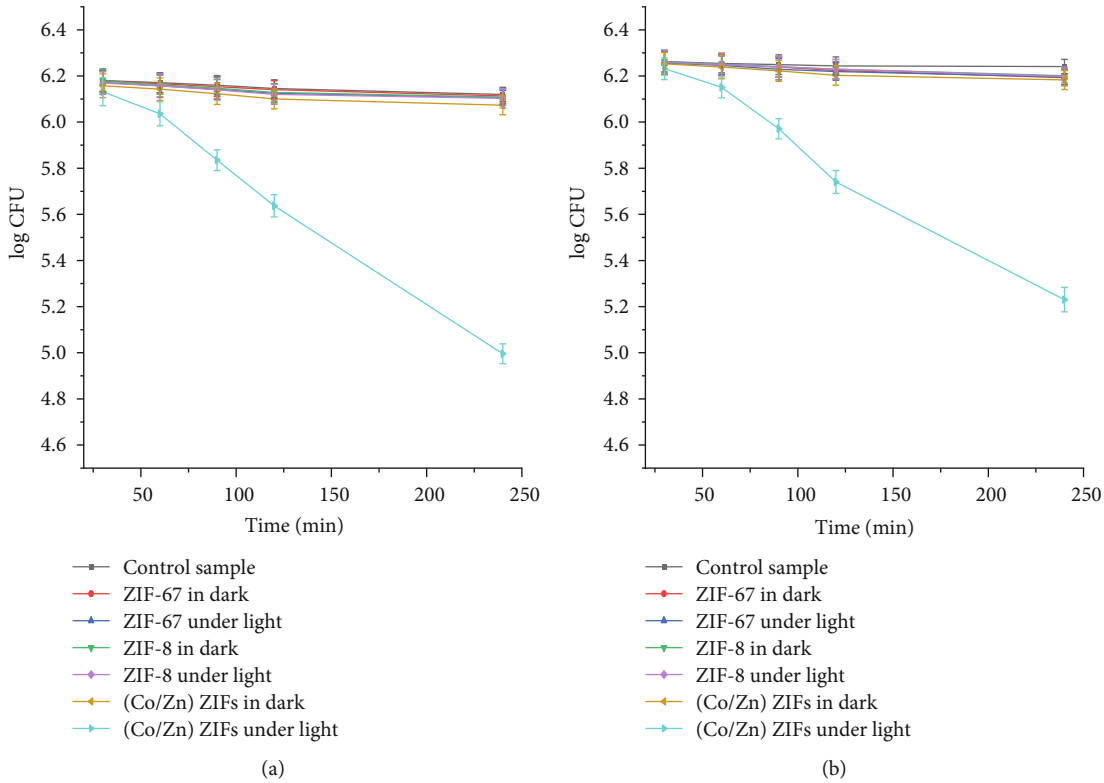

Figure 6: Variation of logarithm of bacterial population of *E. coli* (a) and *S. aureus* (b) with different treatment materials in the dark and under visible-light illumination at different times (each experiment in triplicate).

The adsorption was carried out in the dark for 120 min (to ensure that the adsorption/desorption equilibrium was reached), and then, the light turned up. The TOC data show that ZIF-67, (Co/Zn)ZIFs, and ZIF-8 adsorb a significant amount of RhB in the aqueous solution. The adsorption efficiency of ZIF-67, (Co/Zn)ZIFs, and ZIF-8 is 79.8, 68.7, and 45.6%, respectively (Figure 5(a)). However, ZIF-67 and ZIF-8 do not exhibit any photocatalytic activity under the visible light region. The decreasing TOCs of the solutions treated with ZIF-8 and ZIF-67 are due only to adsorption, whereas (Co/Zn)ZIFs catalyze the degradation of RhB up to 95.5% under illumination. Figure 5(a) shows that TOC decreases from 20.66 to 0.93 $mg{\cdot}L^{-1}$ for the RhB solution treated with (Co/Zn)ZIFs, in which the decrease of 14.19 $mg{\cdot}L^{-1}$ is due to adsorption and 5.54 $mg{\cdot}L^{-1}$ due to photocatalytic degradation.

The leaching experiment was also performed where the catalyst was filtered after 150 min of reaction; the decolorization of RhB almost stopped despite further illumination (Figure 5(c)). This halt indicates that (Co/Zn)ZIF is a heterogeneous catalyst in the photocatalytic degradation of RhB. Because heterogeneous catalysts usually leach the metal ions to the solution, the presence of Zn and Co in the supernatant was detected by using AAS. The results show that a small amount of zinc is present, but cobalt is detected a very small amount in the solution (Table S2). It is possible that the Co-imidazole bond (Co–N) is stronger than the Zn-imidazole bond (Zn–N) because cobalt possesses higher electronegativity (1.88) than zinc (1.65).

The kinetics of the decomposition of RhB on (Co/Zn)ZIFs was studied by using the Hinshelwood–Langmuir model for heterogeneous catalysis at different concentrations in the reduced form as follows:

$$\ln\left(\frac{C_t}{C_0}\right) = -k_r \times t, \tag{4}$$

where k_r is the decomposition rate constant (min^{-1}) and C_0 and C_t are the concentration of RhB at equilibrium in the dark and at time t of photocatalysis. The results (Figure 5(b)) show that the decomposition rate coefficient (k_r) decreases gradually from 0.028 to 0.004 min^{-1} when the RhB concentration increases from 10 to 50 $mg{\cdot}L^{-1}$. RhB at a higher concentration might prevent light from interacting with the catalyst, reducing the photocatalytic efficiency and thus the degradation rate. It is difficult to compare the decomposition rate coefficient because the data are derived from different reaction conditions. However, the k_r value of RhB decomposition in this study is comparable to that of other previously reported studies if the initial concentration is concerned (Table 1).

The antibacterial activity of ZIF materials in an aqueous solution was evaluated by comparing the number of viable bacterial cells after contact with the material with the control sample (without ZIF). Figure 6 shows that ZIF-67 and ZIF-8 have poor antibacterial performance on both *S. aureus* and *E. coli*, with cell survival rates ranging from 87 to 96% with

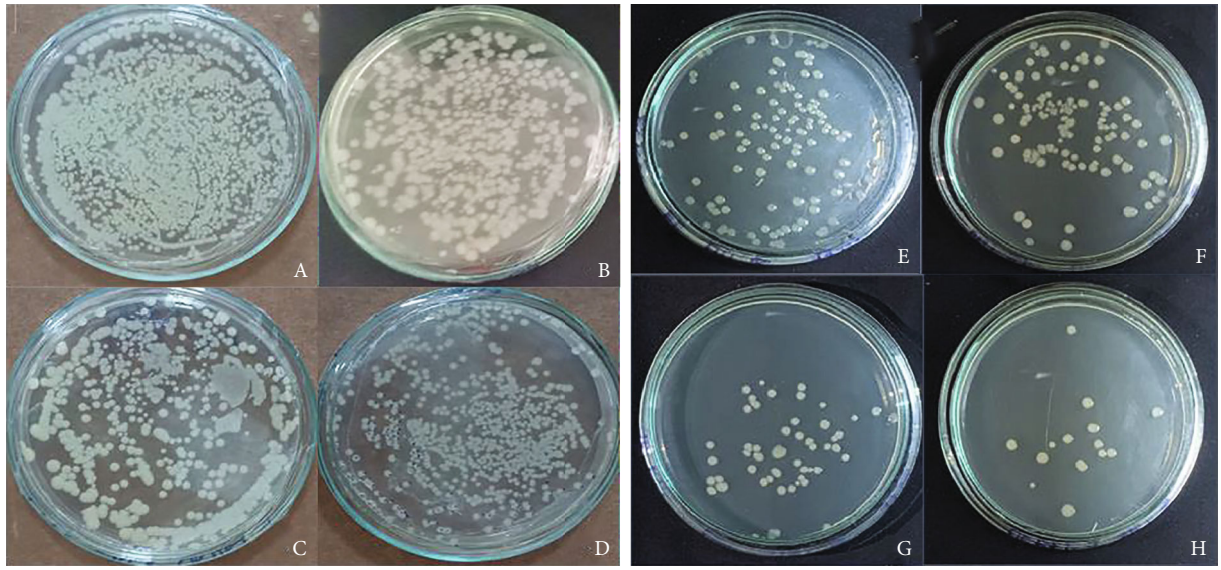

(a) (b)

Figure 7: Cell density of bacterial *E. coli* (a) in the dark (A: control sample, B: 60 min, C: 120 min, and D: 240 min). Cell density of bacterial *E. coli* (b) under illumination (E: control sample, F: 60 min, G: 120 min, and H: 240 min).

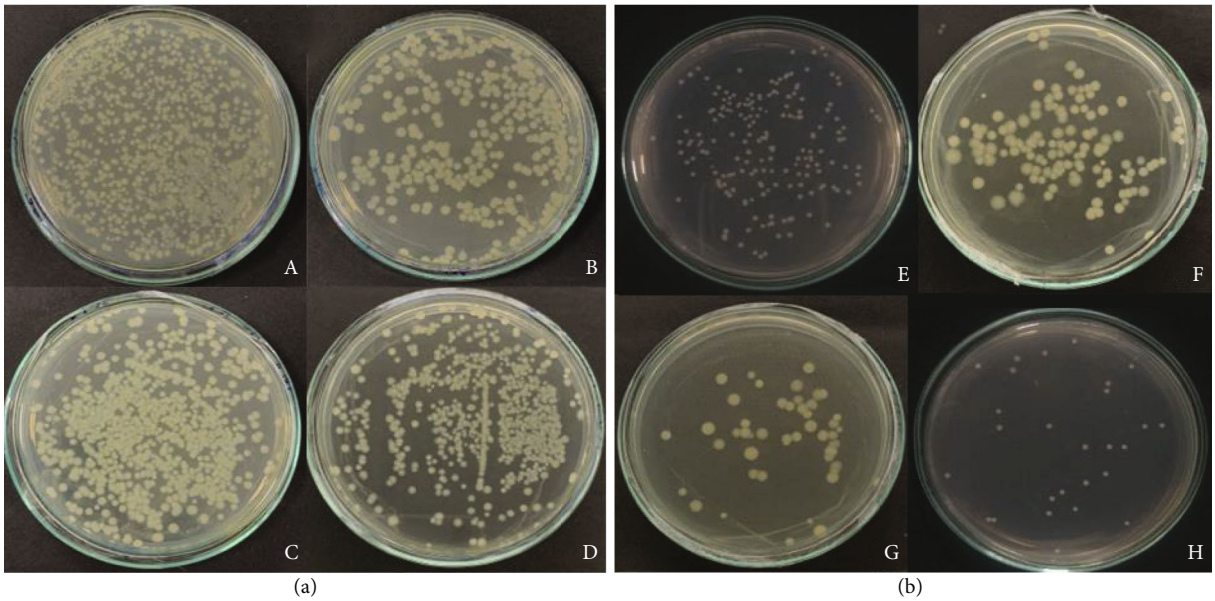

(a) (b)

Figure 8: Cell density of bacterial *S. aureus* (a) in the dark (A: control sample, B: 60 min, C: 120 min, and D: 240 min). Cell density of bacterial *S. aureus* (b) under illumination (E: control sample, F: 60 min, G: 120 min, and H: 240 min).

or without light illumination. However, (Co/Zn)ZIFs have much higher antibacterial activity against both *S. aureus* and *E. coli* without light. Specifically, in the presence of light, (Co/Zn)ZIFs exhibit excellent antibacterial activity on *S. aureus* and *E. coli* strains with a survival rate of 9.14 and 6.68%. The photographs of Petri dishes obtained from *E. coli* and *S. aureus* culture without or with (Co/Zn)ZIFs in the dark and under illumination are shown in Figures 7 and 8. As expected, the *E. coli* and *S. aureus* cultures in the absence of (Co/Zn)ZIFs, *i.e.*, the control samples, continue to grow within four hours (Figures 7(a), 7(e), 8(a), and 8(e)) regardless of lighting or not. The results also show that Gram-negative bacteria *E. coli* are more sensitive to the (Zn/Co)ZIFs than Gram-positive bacteria *S. aureus* because of the difference in their cell membrane structure [34].

Table 2 shows that (Co/Zn)ZIFs have antibacterial activities against Gram-positive and Gram-negative bacteria equivalent to some previously reported materials.

The (Co/Zn)ZIF material is a potential photocatalyst, capable of decolorizing RhB and also inhibiting microorganisms. ZIF-8 and ZIF-67 have large E_g and therefore are not excited under visible light. Combining Zn with Co creates a catalyst with photochemical degradation ability under visible light. This ability of (Co/Zn)ZIFs may result from the

Table 2: A comparison of antibacterial activity of (Co/Zn)ZIF with other materials reported previously.

Materials	Bacterial strains	Antibacterial activity	References
RFP&o-NBA@ZIF-8	*E. coli*	Inhibition rate of 95% against *E. coli* under light condition during 12 hours	[35]
MOF-53(Fe)/Van	*S. aureus*	Inhibition rate of 99.3% against *S. aureus* at concentration 200 $\mu g \cdot mL^{-1}$ of MOF-53(Fe)/Van	[36]
HKUST-1/OCBs	*E. coli*	Growth inhibition of bacteria: 90.2%	[37]
CP/CNF/ZIF-67	*E. coli*	Antibacterial rate reached 80%	[38]
WO_{3-X}	*E. coli* and *S. aureus*	Inhibition rate of 100% against *E. coli* and *S. aureus* at 100 $\mu g \cdot mL^{-1}$ after six hours of contact	[39]
(Co/Zn)ZIFs	*E. coli* and *S. aureus*	Inhibition rate 90.86% against *S. aureus* and 93.8% against *E. coli* after four hours of contact under visible light condition	The present study

addition of Zn to the intermediate band formation between the conduction (CB) and valence (VB) regions of ZIF-67 and ZIF-8. Visible light can excite electrons from VB, and an energy state adds to the Co3d level to CB, causing electron formation (e^-) and photogenerated hole (h^+). The e^-/h^+ pair initiates the reduction or oxidation of O_2 and H_2O in the solution to generate free radicals. These free radicals oxidize organic pollutants to form mineral products. The photocatalytic reaction can occur as follows:

$$\begin{gathered}\left(\frac{\mathrm{Co}}{\mathrm{Zn}}\right)\mathrm{ZIFs} + h\nu \longrightarrow \left(\frac{\mathrm{Co}}{\mathrm{Zn}}\right)\mathrm{ZIFs}\left(\frac{\mathrm{h}^+}{\mathrm{e}^-}\right)\\ \mathrm{e}^- + \mathrm{O}_2 \longrightarrow \mathrm{O}_2{}^{*-}\\ \left(\frac{\mathrm{Co}}{\mathrm{Zn}}\right)\mathrm{ZIFs}\left(\mathrm{h}^+\right) + \mathrm{H}_2\mathrm{O} \longrightarrow {}^{\cdot}\mathrm{OH} + \mathrm{H}^+ + \left(\frac{\mathrm{Co}}{\mathrm{Zn}}\right)\mathrm{ZIFs}\left(\mathrm{h}^+\right)\\ \frac{{}^{\cdot}\mathrm{OH}}{\mathrm{O}_2{}^{*-}} + \mathrm{RhB} \longrightarrow \text{Decomposition products}\end{gathered} \tag{5}$$

The free radicals ${}^{\cdot}OH/O_2{}^{*-}$ can oxidize and damage cell membranes, organelles, and bacterial DNA, resulting in the destruction of bacteria. This pathway is also considered one of many materials' principal bactericidal mechanisms, as reported in previous studies [8–12, 34, 40–43].

4. Conclusion

The ZIF-8, ZIF-67, and (Zn/Co)ZIF materials synthesized with the solvothermal method have uniform morphology with a large surface area. Under visible light, (Zn/Co)ZIFs exhibit high photocatalytic activity toward the RhB degradation and, simultaneously, inhibit *E. coli* and *S. aureus*, while ZIF-8 and ZIF-67 do not. The synergistic system ZIF-67/ZIF-8 for simultaneous dye degradation and bacteria inhibition suggests a new approach for developing multifunctional materials for environmental treatments.

Data Availability

The data used to support the findings of this study are available from the corresponding authors upon request.

Conflicts of Interest

The authors declare that they have no conflicts of interest.

Acknowledgments

This study was financially supported by the Van Lang University, Vietnam.

Supplementary Materials

Table S1: the (Co/Zn)ZIF sample with Co/Zn molar ratio of 6/4 presents highest photocatalytic and antibacterial activity; therefore, this material was selected for further experiments. Table S2: metal elements were leached out but a small amount of zinc is present, but cobalt is detected a very small amount. *(Supplementary Materials)*

References

[1] M. Rafatullah, O. Sulaiman, R. Hashim, and A. Ahmad, "Adsorption of methylene blue on low-cost adsorbents: a review," *Journal of Hazardous Materials*, vol. 177, no. 1-3, pp. 70–80, 2010.

[2] K.-T. Chung, "Azo dyes and human health: a review," *Journal of Environmental Science and Health, Part C*, vol. 34, no. 4, pp. 233–261, 2016.

[3] K. Golka, S. Kopps, and Z. W. Myslak, "Carcinogenicity of azo colorants: influence of solubility and bioavailability," *Toxicology Letters*, vol. 151, no. 1, pp. 203–210, 2004.

[4] S. Ghoreishi and R. Haghighi, "Chemical catalytic reaction and biological oxidation for treatment of non-biodegradable textile effluent," *Chemical Engineering Journal*, vol. 95, no. 1-3, pp. 163–169, 2003.

[5] S. Chatterjee, M. W. Lee, and S. H. Woo, "Adsorption of Congo red by chitosan hydrogel beads impregnated with carbon nanotubes," *Bioresource Technology*, vol. 101, no. 6, pp. 1800–1806, 2010.

[6] E. Lorenc-Grabowska and G. Gryglewicz, "Adsorption characteristics of Congo red on coal-based mesoporous activated carbon," *Dyes and Pigments*, vol. 74, no. 1, pp. 34–40, 2007.

[7] I. D. Mall, V. C. Srivastava, N. K. Agarwal, and I. M. Mishra, "Removal of congo red from aqueous solution by bagasse fly ash and activated carbon: kinetic study and equilibrium isotherm analyses," *Chemosphere*, vol. 61, no. 4, pp. 492–501, 2005.

[8] C.-H. Liu, J.-S. Wu, H.-C. Chiu, S.-Y. Suen, and K. H. Chu, "Removal of anionic reactive dyes from water using anion exchange membranes as adsorbers," *Water Research*, vol. 41, no. 7, pp. 1491–1500, 2007.

[9] J.-S. Wu, C.-H. Liu, K. H. Chu, and S.-Y. Suen, "Removal of cationic dye methyl violet 2B from water by cation exchange membranes," *Journal of Membrane Science*, vol. 309, no. 1-2, pp. 239–245, 2008.

[10] U. G. Akpan and B. H. Hameed, "Parameters affecting the photocatalytic degradation of dyes using TiO2-based photocatalysts: a review," *Journal of Hazardous Materials*, vol. 170, no. 2-3, pp. 520–529, 2009.

[11] K. Rajeshwar, M. Osugi, W. Chanmanee et al., "Heterogeneous photocatalytic treatment of organic dyes in air and aqueous media," *Journal of Photochemistry and Photobiology C: Photochemistry Reviews*, vol. 9, no. 4, pp. 171–192, 2008.

[12] J. L. Wang and L. J. Xu, "Advanced oxidation processes for wastewater treatment: formation of hydroxyl radical and application," *Critical Reviews in Environmental Science and Technology*, vol. 42, no. 3, pp. 251–325, 2012.

[13] M. G. Nair, M. Nirmala, K. Rekha, and A. Anukaliani, "Structural, optical, photo catalytic and antibacterial activity of ZnO and Co doped ZnO nanoparticles," *Materials Letters*, vol. 65, no. 12, pp. 1797–1800, 2011.

[14] D. Valerini, L. Tammaro, R. Vitali, G. Guillot, and A. Rinaldi, "Sputter-deposited Ag nanoparticles on electrospun PCL scaffolds: morphology, wettability and antibacterial activity," *Coatings*, vol. 11, no. 3, p. 345, 2021.

[15] S. Rao, Y. Li, H. Liu et al., "Polyethyleneimine induced highly dispersed Ag nanoparticles over g-C_3N_4 nanosheets for efficient photocatalytic and antibacterial performance," *Ceramics International*, vol. 47, no. 6, pp. 8528–8537, 2021.

[16] L. Zhao, H.-H. Wu, C. Yang et al., "Mechanistic origin of the high performance of Yolk@Shell Bi_2S_3@N-doped carbon nanowire electrodes," *ACS Nano*, vol. 12, no. 12, pp. 12597–12611, 2018.

[17] K. Zhou, B. Mousavi, Z. Luo, S. Phatanasri, S. Chaemchuen, and F. Verpoort, "Characterization and properties of Zn/Co zeolitic imidazolate frameworks vs. ZIF-8 and ZIF-67," *Journal of Materials Chemistry A*, vol. 5, no. 3, pp. 952–957, 2017.

[18] K. T. Butler, C. H. Hendon, and A. Walsh, "Designing porous electronic thin-film devices: band offsets and heteroepitaxy," *Faraday Discussions*, vol. 201, pp. 207–219, 2017.

[19] M.-H. Chen, Q.-Y. Lu, Y.-M. Li, M.-M. Chu, and X.-B. Cao, "ZnO@ZIF-8 core–shell heterostructures with improved photocatalytic activity," *CrystEngComm*, vol. 23, no. 24, pp. 4327–4335, 2021.

[20] H. Yang, X.-W. He, F. Wang, Y. Kang, and J. Zhang, "Doping copper into ZIF-67 for enhancing gas uptake capacity and visible-light-driven photocatalytic degradation of organic dye," *Journal of Materials Chemistry*, vol. 22, no. 41, pp. 21849–21851, 2012.

[21] M. Taheri, D. Ashok, T. Sen et al., "Stability of ZIF-8 nanopowders in bacterial culture media and its implication for antibacterial properties," *Chemical Engineering Journal*, vol. 413, article 127511, 2021.

[22] N. T. T. Tu, P. C. Sy, T. T. Minh et al., "Synthesis of (Zn/Co)-based zeolite imidazole frameworks and their applications in visible light-driven photocatalytic degradation of Congo red," *Journal of Inclusion Phenomena and Macrocyclic Chemistry*, vol. 95, no. 1-2, pp. 99–110, 2019.

[23] N. T. T. Tu, T. V. Thien, P. D. Du, V. T. T. Chau, T. X. Mau, and D. Q. Khieu, "Adsorptive removal of Congo red from aqueous solution using zeolitic imidazolate framework–67," *Journal of Environmental Chemical Engineering*, vol. 6, no. 2, pp. 2269–2280, 2018.

[24] G. Zhong, D. Liu, and J. Zhang, "The application of ZIF-67 and its derivatives: adsorption, separation, electrochemistry and catalysts," *Journal of Materials Chemistry A*, vol. 6, no. 5, pp. 1887–1899, 2018.

[25] Z.-X. Y. J. Low, J. Yao, Q. Liu et al., "Crystal transformation in zeolitic-imidazolate framework," *Crystal Growth & Design*, vol. 14, no. 12, pp. 6589–6598, 2014.

[26] Y. Li, K. Zhou, M. He, and J. Yao, "Synthesis of ZIF-8 and ZIF-67 using mixed-base and their dye adsorption," *Microporous and Mesoporous Materials*, vol. 234, pp. 287–292, 2016.

[27] Q. Luo, X. Huang, Q. Deng et al., "Novel 3D cross-shaped Zn/Co bimetallic zeolite imidazolate frameworks for simultaneous removal Cr (VI) and Congo Red," *Environmental Science and Pollution Research*, vol. 29, no. 26, pp. 40041–40052, 2022.

[28] S. Bordiga, C. Lamberti, G. Ricchiardi et al., "Electronic and vibrational properties of a MOF-5 metal–organic framework: ZnO quantum dot behaviour," *Chemical Communications*, vol. 20, pp. 2300-2301, 2004.

[29] T. N. Nguyen, H. P. Nguyen, T.-H. Kim, and S. W. Lee, "Bimetallic Co/Zn-ZIF as an efficient photocatalyst for degradation of indigo carmine," *Korean Journal of Materials Research*, vol. 28, no. 1, pp. 68–74, 2018.

[30] R. Ran, J. G. McEvoy, and Z. Zhang, "Synthesis and optimization of visible light active $BiVO_4$ photocatalysts for the degradation of RhB," *International Journal of Photoenergy*, vol. 2015, Article ID 612857, 14 pages, 2015.

[31] A. H. Kianfar, M. A. Arayesh, and M. M. Momeni, "Degradation of MB and RhB by modified ZrO_2 nanoparticles via sunlight," *Applied Physics A*, vol. 127, no. 2, pp. 1–9, 2021.

[32] N. Kumaresan, M. M. A. Sinthiya, K. Ramamurthi, R. R. Babu, and K. Sethuraman, "Visible light driven photocatalytic activity of ZnO/CuO nanocomposites coupled with rGO heterostructures synthesized by solid-state method for RhB dye degradation," *Arabian Journal of Chemistry*, vol. 13, no. 2, pp. 3910–3928, 2020.

[33] R. Uma, K. Ravichandran, S. Sriram, and B. Sakthivel, "Cost-effective fabrication of ZnO/g-C_3N_4 composite thin films for enhanced photocatalytic activity against three different dyes (MB, MG and RhB)," *Materials Chemistry and Physics*, vol. 201, pp. 147–155, 2017.

[34] L. Wang, C. Hu, and L. Shao, "The antimicrobial activity of nanoparticles: present situation and prospects for the future," *International Journal of Nanomedicine*, vol. 12, pp. 1227–1249, 2017.

[35] Z. Song, Y. Wu, Q. Cao, H. Wang, X. Wang, and H. Han, "pH-responsive, light-triggered on-demand antibiotic release from functional metal-organic framework for bacterial infection combination therapy," *Advanced Functional Materials*, vol. 28, no. 23, article 1800011, 2018.

[36] S. Lin, X. Liu, L. Tan et al., "Porous iron-carboxylate metal–organic framework: a novel bioplatform with sustained antibacterial efficacy and nontoxicity," *ACS Applied Materials & Interfaces*, vol. 9, no. 22, pp. 19248–19257, 2017.

[37] C. Duan, X. Meng, C. Liu et al., "Carbohydrates-rich corncobs supported metal-organic frameworks as versatile biosorbents for dye removal and microbial inactivation," *Carbohydrate Polymers*, vol. 222, article 115042, 2019.

[38] L. Qian, D. Lei, X. Duan et al., "Design and preparation of metal-organic framework papers with enhanced mechanical properties and good antibacterial capacity," *Carbohydrate Polymers*, vol. 192, pp. 44–51, 2018.

[39] C. Bankier, R. Matharu, Y. Cheong, G. Ren, E. Cloutman-Green, and L. Ciric, "Synergistic antibacterial effects of metallic nanoparticle combinations," *Scientific Reports*, vol. 9, no. 1, pp. 1–8, 2019.

[40] W. Wang, K. J. Lu, C. H. Yu, Q. L. Huang, and Y. Z. Du, "Nano-drug delivery systems in wound treatment and skin regeneration," *Journal of nanobiotechnology*, vol. 17, no. 1, pp. 1–15, 2019.

[41] D. Liu, Y. Chen, F. Ding et al., "Simultaneous production of butanol and acetoin by metabolically engineered Clostridium acetobutylicum," *Metabolic Engineering*, vol. 27, pp. 107–114, 2015.

[42] B. Ahmed, A. K. Ojha, A. Singh et al., "Well-controlled in-situ growth of 2D WO_3 rectangular sheets on reduced graphene oxide with strong photocatalytic and antibacterial properties," *Journal of Hazardous Materials*, vol. 347, pp. 266–278, 2018.

[43] M. M. Khan, S. Kumar, T. Ahamad, and A. N. Alhazaa, "Enhancement of photocatalytic and electrochemical properties of hydrothermally synthesized WO_3 nanoparticles via Ag loading," *Journal of Alloys and Compounds*, vol. 743, pp. 485–493, 2018.